Available online at www.eccomasproceedia.org
Eccomas Proceedia COMPDYN (2025) 2323-2334

ECCOMAS
Proceedia

COMPDYN 2025
10th ECCOMAS Thematic Conference on
Computational Methods in Structural Dynamics and Earthquake Engineering
M. Papadrakakis, M. Fragiadakis (eds.)
Rhodes Island, Greece, 15-18 June 2025

NUMERICAL EVALUATION OF THE SEISMIC PERFORMANCE OF BRIDGES MADE OF UHPC AND TITANIUM ALLOY REINFORCING BARS

Luis A. Bedriñana[1], Jorge Atusparia[1], Heider Mendoza[1], Mahesh Acharya[2], and Mustafa Mashal[2]

[1] Universidad de Ingenieria y Tecnologia - UTEC
Jr. Medrano Silva 165, Barranco, Lima, Peru
e-mail: lbedrinana@utec.edu.pe, jorge.atusparia@utec.edu.pe, hmendozap@utec.edu.pe

[2] Idaho State University
Pocatello, ID, United States
maheshacharya@isu.edu, mashmust@isu.edu

Abstract

Conventional Reinforced concrete (RC) structures, typically engineered for a lifespan of 50 years, are susceptible to various deterioration issues. In particular, continuous deterioration can weaken the structural elements of bridges in coastal areas, potentially reducing their lifespan. To address this issue, bridge engineers have proposed the use of advanced materials like ultra-high-performance concrete, titanium alloy reinforcement, composite materials, and others. Recently, the combination of titanium alloy bars (TiABs) and ultra-high-performance concrete (UHPC), namely TARUHPC structures, has been proposed as a novel construction method to enhance the durability and longevity of RC bridges in seismic regions. However, the seismic performance of TARUHPC is not fully characterized yet. Thus, it is important to assess the seismic deformation capacity of TARUHPC bridges. This paper evaluates the seismic performance of TARUHPC piers via nonlinear Finite Element (FE) models. Fiber-based models with distributed plasticity were developed to evaluate three scenarios: (1) normal concrete with TiABs (NC-TI), (2) UHPC with conventional steel (U-TI), and (3) TARUHPC. The parameters of the models were fine-tuned through model updating based on previous experimental cyclic tests. After a detailed validation, the FE models were able to capture the ductility, stiffness degradation, residual deformation, energy dissipation, and failure modes observed in the test specimens. Moreover, a detailed parametric analysis is conducted to explore the influence of different design variables on the seismic performance of TARUHPC bridges. Finally, some important design recommendations are provided.

Keywords: UHPC, titanium alloy bars, cyclic behavior, FE analysis, fiber elements.

ISSN:2623-3347
Peer-review under responsibility of the organizing committee of COMPDYN 2025.
doi: 10.7712/120125.12569.24856

1 INTRODUCTION

Conventional Reinforced Concrete (RC) structures, typically engineered for a lifespan of 50 years, are susceptible to various deterioration issues such as alkali-aggregate reactions, chemical attacks, freeze-thaw cycles, reinforcement corrosion, and fire damage [1]. In particular for bridges in coastal areas, the continuous deterioration of concrete elements can reduce their safety, potentially reducing their lifespan. For instance, in the United States, there are more than 620,000 bridges across the nation, and around 6.8% of the total existing bridges are classified as structurally deficient [2], evidencing the serious issue of deterioration. This issue has motivated researchers to evaluate the application of advanced materials like ultra-high-performance concrete, titanium alloy reinforcement, high-strength steel, composite materials, and improved coatings for more durable bridges. In this line, the combination of titanium alloy bars (TiABs) with ultra-high-performance concrete (UHPC), namely TARUHPC, has been recently proposed as an attractive construction method for more durable RC bridges in seismic regions [3, 4]. TiABs for construction applications have been previously investigated [5, 6], showing that TiABs offer excellent deformation capacity, superior strength, lower fatigue potential, reduced density, decreased corrosion susceptibility, and minimal residual deformations compared to standard steel. On the other hand, UHPC is an advanced cementitious composite material with mechanical and durability properties significantly superior to conventional concrete [7]. UHPC, which is comprised of Portland cement, fine aggregate, silica fume, water-reducing additives, and steel microfibers [8], offers high strength, ductility, durability, and low porosity [9]. Recently, the mechanical behavior of TARUHPC structures has been evaluated [10]. Despite these advancements, the practical application of TARUHPC in bridge engineering is limited due to the lack of information on their seismic performance.

This paper evaluates the seismic performance of TARUHPC piers, expanding on previous experimental work [10], by conducting a detailed numerical research of test specimens. A parametric analysis is also conducted to study the failure mode, hysteretic characteristics, displacement ductility, energy dissipation, and stiffness degradation of TARUHPC piers. Finally, design recommendations are provided.

2 EXPERIMENTAL EVALUATION OF TARUHPC PIERS

This paper discusses three types of bridge piers, previously tested by Acharya et al. [3, 10], and Figure 1 indicates their main features. All the pier specimens had a cross-section of 200mm x 200mm and a total height of 1350mm. The first specimen (NC-TI) is made of normal concrete with four D16 (#5) TiABs as longitudinal reinforcement. The second specimen (U-NS) consisted of UHPC reinforced with six D16 (#5) conventional Grade-60 steel rebars. The third specimen (U-TI) was made of UHPC reinforced with four D16 TiABs. Confining reinforcement in the NC-TI and U-TI specimens consisted of D10 (#3) TiABs for hoops, spaced at 10mm vertically. As for the U-NS specimen, the confinement consisted of D10 hoops made of Grade-60 conventional steel, spaced also at 10mm. Pseudo-threaded TiABs and proprietary UHPC were used for this research. Mechanical properties of the concrete and reinforcing used in the specimens are listed in Table 1 and Table 2, respectively.

A constant vertical axial load of 71.17kN was applied to each specimen, corresponding to an axial load ratio of 0.056 for the NC-TI specimen and 0.014 for both the U-NS and U-TI specimens. Fully reversed, quasi-static, cyclic lateral loads were applied to the specimens. The testing of all specimens continued until the piers were close to collapse. However, for the purposes of this study, it will be assumed that the ultimate state of the specimens occurred when a degradation of 15%, or larger, of the peak strength was reached in any loading direction. More detailed information on the test and test results are reported elsewhere [3, 10].

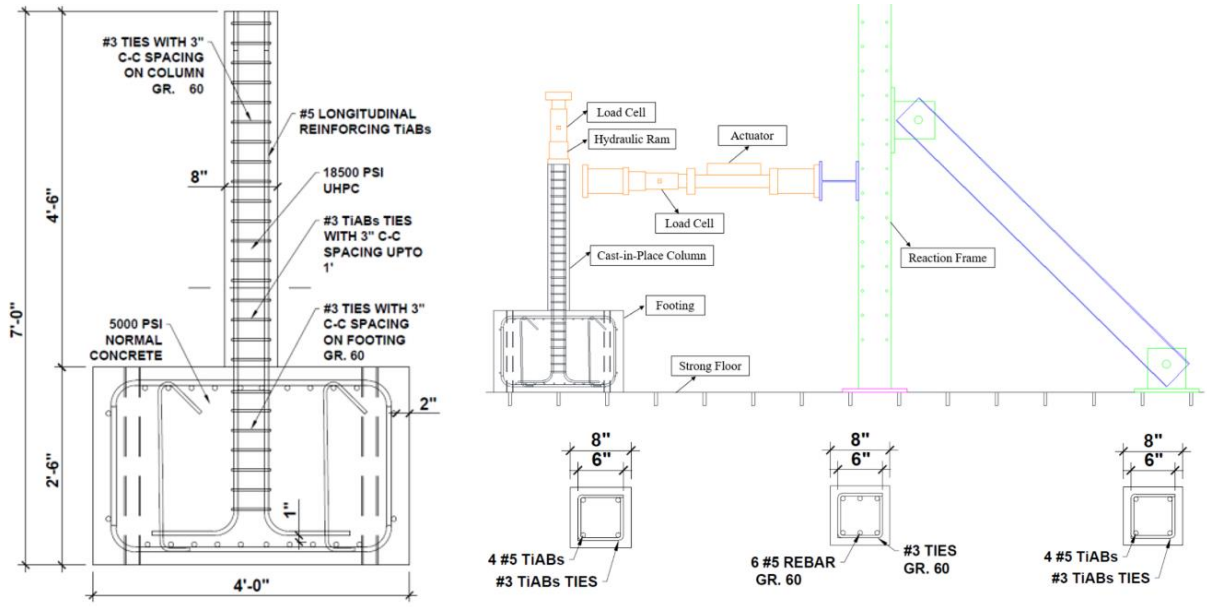

Figure 1: Detail of piers specimens. Dimensions in (ft and inch); 1 inch = 25.4 mm; 1 ft = 0.305 m. After [3, 10].

Specimen	Structural element	Compressive strength (MPa)		Tensile strength (MPa)	
		28 days	Test Day	28 days	Test Day
NC-TI	Foundation	35.87	47.13	2.29	3.42
	Pier	36.30	47.97	2.30	3.08
U-NS	Foundation	25.32	34.69	1.55	1.79
	Pier	100.88	130.43	16.28	18.06
U-TI	Foundation	35.87	47.13	2.29	3.43
	Pier	124.88	130.11	15.37	18.18

Table 1: Measured mechanical properties of concrete materials.

Reinforcement type	Yield Strength (MPa)	Ultimate strength (MPa)	Elastic modulus (MPa)
Titanium Alloy Bars	965.00	1035.00	103421.00
Grade-60 bars	420.00	620.00	200000.00

Table 2: Material properties (specified) of reinforcing bars.

3 NUMERICAL MODELS FOR TARUHPC PIERS

Nonlinear finite element (FE) models of the test specimens were developed using the OpenSees platform [9]. Figure 2 shows the main features of the three numerical models developed in this study, based on the dimensions and reinforcement layout of the test specimens described in the previous section. The cross-section of each specimen was appropriately divided into reinforcing material, unconfined cover concrete, and confined core concrete fibers (see Figure 2) according to the actual geometry of test specimens. The reinforcement in the section was considered as perfectly bonded with the concrete. Confinement in the core concrete was considered indirectly by incrementing the compressive strength and deformation capacity of that concrete. Displacement-based nonlinear beam-column elements were used to model the piers, combined with the Legendre integration scheme. The main pier of all speci-

mens was modeled with 5 equal-length beam-column elements, while the foundation was modeled with three 3 equal-length beam-column elements (only for specimens U-NS and U-TI). Each beam-column element contained 5 integration points. Note that in specimen NC-TI it was not necessary to model the foundation as the damage concentrated only in the main pier. Other boundary conditions were similar as in the test specimens.

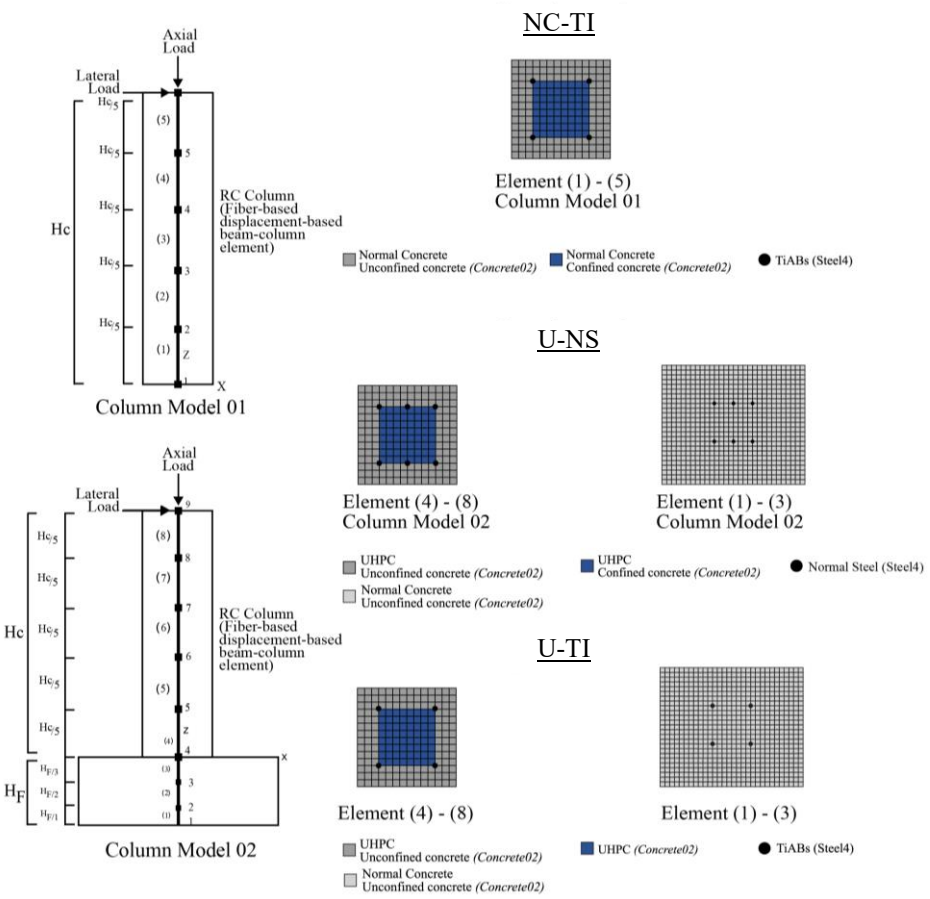

Figure 2: Schematics of fiber-based models for the test specimens.

Appropriate constitutive models were selected from the OpenSees library. The conventional concrete material was modeled with the Concrete02 library, which is based on the Kent-Park model [12]. The confinement effects were considered using the Mander model [13] for confined concrete. As for the constitutive model of UHPC, the approach of Wang et al. [14] was used to modify the Concrete02 library to account for the steel fiber content. The Concrete01 library with zero tension was used to represent the concrete in the foundation (for some specimens). The stress-strain behavior of conventional Grade-60 steel rebars and TiABs was modeled by the Steel4 library, which combines kinematic and isotropic hardening [15]. The main characteristics of the materials models were determined according to the material properties listed in Table 1 and Table 2. The lateral load in the FE models was applied at the height of the actuator, which was 984.25 mm from the pier's bottom. The constant axial load was applied at the top node of the models. Moreover, the cyclic loading history in the FE analyses was consistent with the test conditions.

Figure 3 compares the hysteretic curves obtained from the FE analysis with the experimental curves for the three specimens. Moreover, Table 3 compares the test and numerical results in terms of the peak lateral strength (F_m). As shown in Figure 3, the hysteretic curves

are in good agreement with test results, so the numerical models were able to estimate the hysteretic shape, energy dissipation, residual displacement, and strength degradation with significant accuracy. As seen in Table 3, the strength prediction is within adequate range. Nonetheless, a minor discrepancy was noted for specimen U-NS in the negative loading part of the curve for larger drifts (after 4%), which is associated with the significant concrete damage noted on the top surface of the foundation. For specimens NC-TI, it was noted that the concrete was damaged before the yielding of TiABs so this reinforcement was almost elastic (see hysteretic curve). For specimen U-TI, the TiABs were below their tensile strength, but they developed larger stresses due to the presence of UHPC.

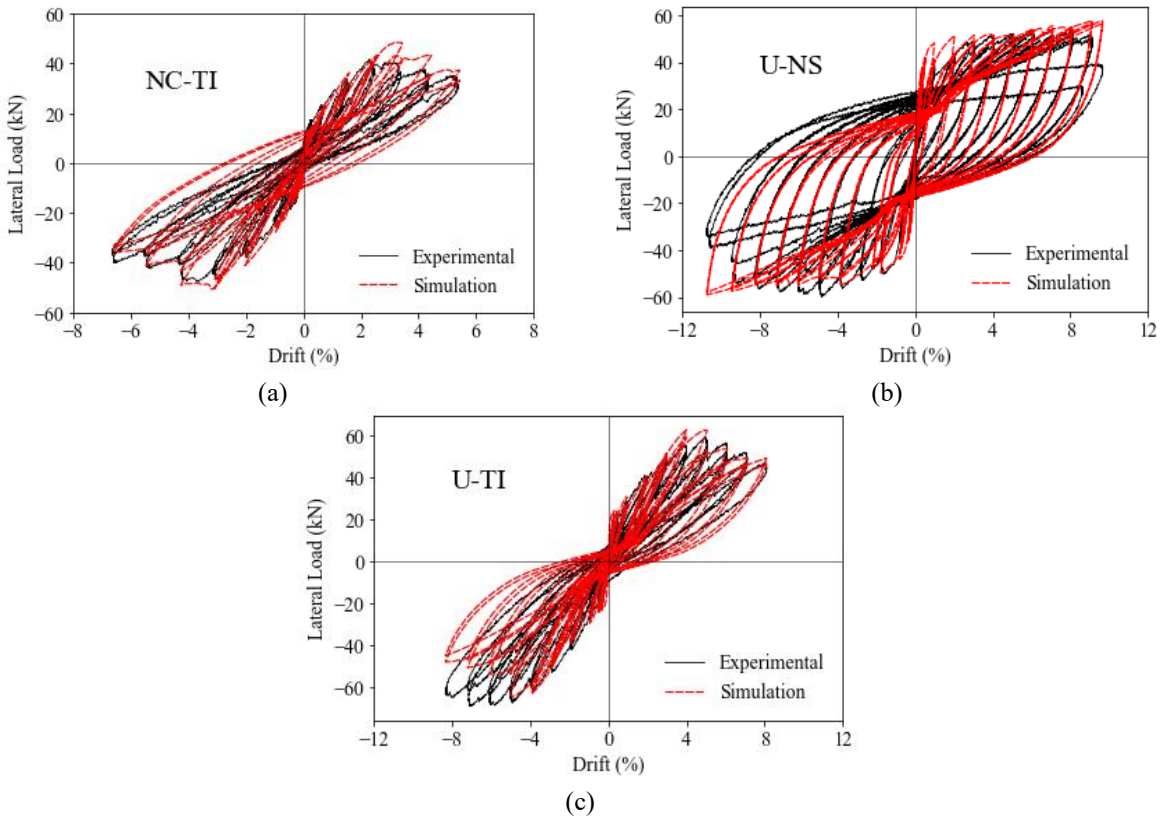

Figure 3: Comparison between experimental and calculated load-deformation response for (a) NC-TI, (b) U-NS, and (c) U-TI specimens.

Specimen	Peak strength (kN)		
	Test	FE models	FEM/test
NC-TI	50.0	43.7	0.9
U-NS	48.0	57.0	1.2
U-TI	59.0	59.8	1.0

Table 3: Lateral strength prediction of pier specimens.

Figure 4 and Figure 5 show the variation of cumulative energy and residual displacement, respectively for each loading cycle. For clarity, only the results of the positive loading are presented. The FE models were accurate in predicting the cumulative energy for specimens U-NS and U-TI, whereas some discrepancies were noted in specimen NC-TI. The discrepancies can be associated with the difficulty of the model to capture the onset of cover concrete spalling for normal concrete. It was also noted that NC-TI dissipated less energy than the oth-

er specimens due to the normal concrete reaching its strength before the yielding of TiABs. The specimen U-NS dissipated the largest amount of energy due to the extensive yielding of normal steel bars. The FE models were also able to predict the residual drifts at low peak drifts for all the specimens; however, at large deformations, some discrepancies were noted. In particular, the largest discrepancies were observed in specimen NC-TI due to the extent of concrete damage. Therefore, the FE models showed high accuracy in predicting the seismic response of the specimens.

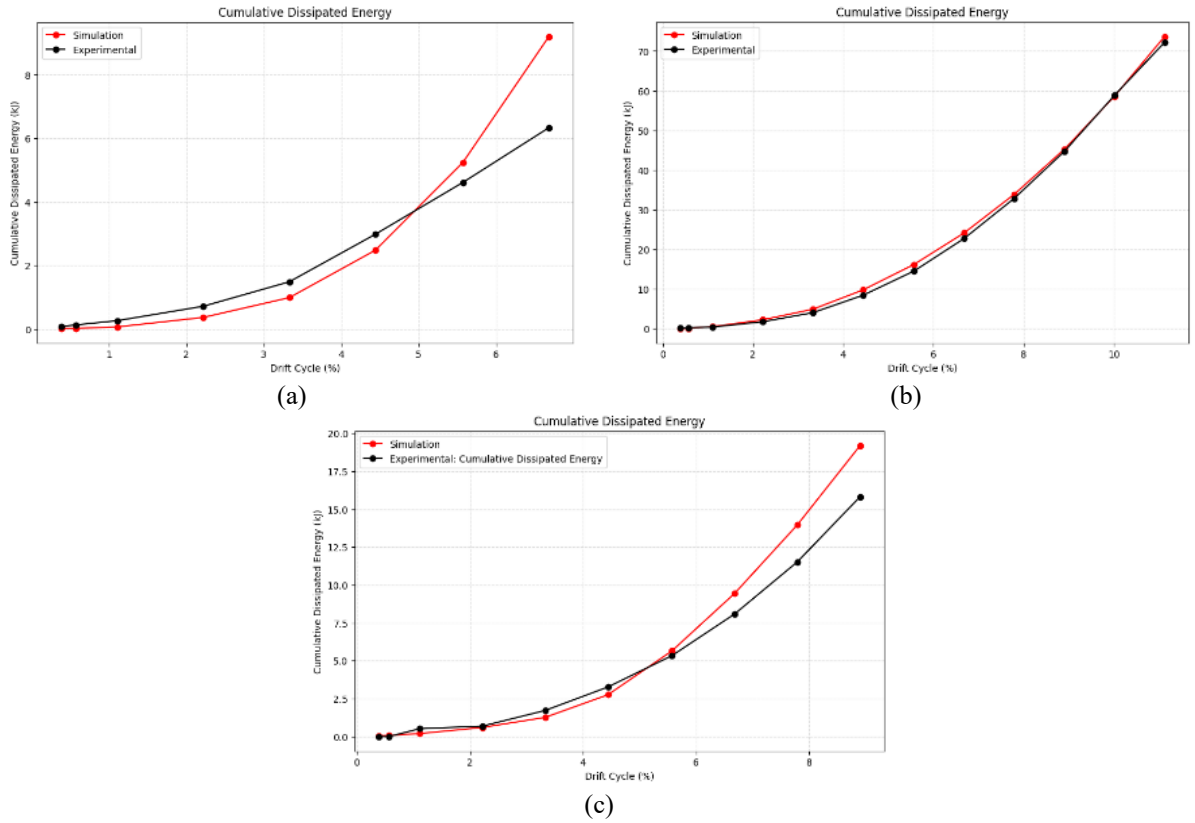

Figure 4: Comparison of observed and calculated cumulative dissipated Energy for (a) NC-TI, (b) U-NS, and (c) U-TI specimens.

4 PARAMETRIC ANALYSIS OF TARUHPC STRUCTURES

4.1 Influence of axial loads

With the previously validated FE models, a parametric study was performed to study the residual drift and damping ratio of the three types of piers described in previous sections. The first parameter evaluated in this study is the axial load. For the NC-TI specimen, different axial loads were applied with the following values 30, 50, 70, 90, and 110kN, which resulted in the following axial load ratios (η) of 0.021, 0.035, 0.049, 0.063, and 0.077. For specimens U-NS and U-TI, the axial loads were set to 70, 150, 230, 310, and 390kN, corresponding to values of η of 0.013, 0.028, 0.044, 0.059, and 0.074.

Figure 6 shows the variation of residual drift for different values of η for the three specimens. For specimen NC-TI (see Figure 6(a)), the residual drift slowly increases with the lateral drifts until reaching a drift of around 3%, after which the residual drift drastically increases. These sudden increments of residual drifts can be attributed to the concrete spalling and damage on the confined concrete before the TiABs reach their yield strength. Moreover,

the residual drift seems to be insensitive to the increments of axial load for this specimen as the concrete fails prematurely. The largest residual drifts noted in this specimen were above 2.0%. A similar trend was noted for specimen U-TI (TARUHPC); however, the sudden increments of residual drifts occurred after 5% drifts. Moreover, the increments of axial load in U-TI reduced the magnitude of residual drift because the UHPC can sustain larger compressive deformations compared to normal concrete. For specimen U-NS (See Figure 6(b)), the residual drift remains relatively constant and close to 0% until reaching a peak drift of 1.5%, after which, it rapidly grows with increments of lateral deformation. The influence of axial loading becomes more notorious for lateral drifts exceeding 4%, as the increments on axial loads reduced the residual drifts in this specimen.

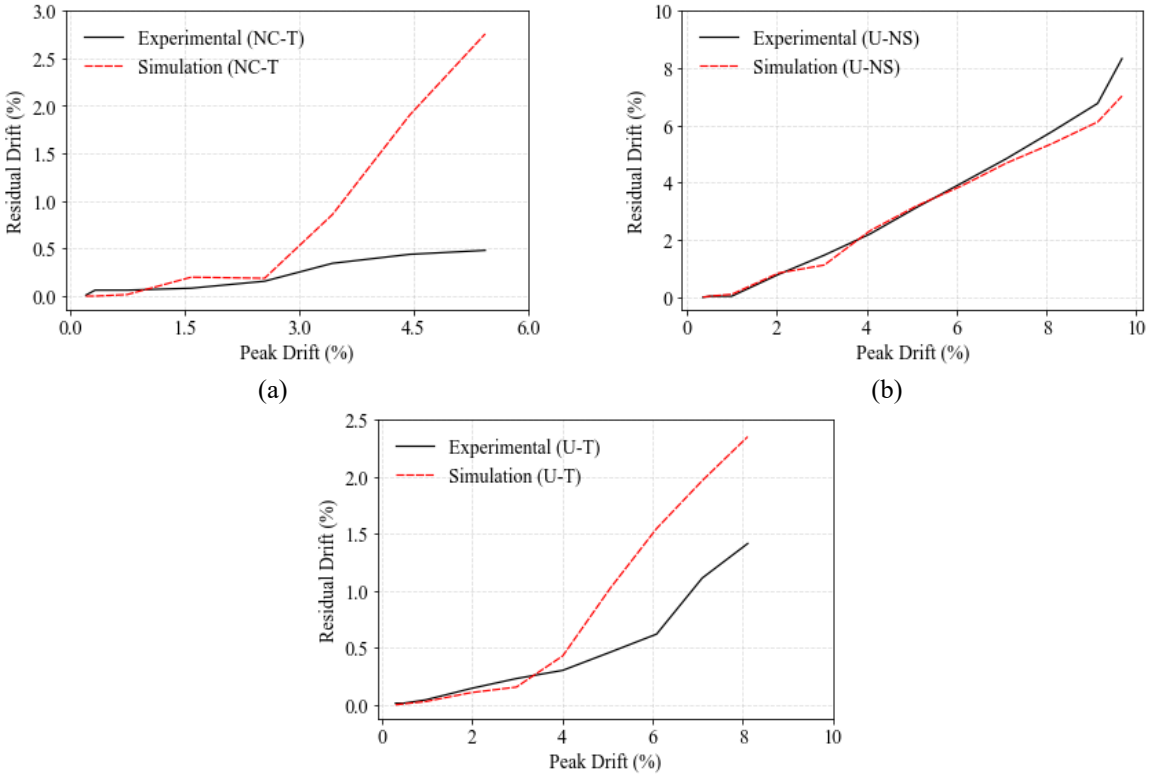

Figure 5: Comparison of observed and calculated residual drift for (a) NC-TI, (b) U-NS, and (c) U-TI specimens.

Figure 7 shows the influence of axial loads in the equivalent damping ratio of the specimens. As noted in Figure 7 (a) and (c), the impact of axial load on the damping was minor for specimens NC-TI and U-TI. These types of piers exhibit a similar trend of damping as the damping remained below 4% when the lateral drift was less than 2.5%, followed by a drastic increment of damping superior. It is worth noting that these values of equivalent damping ratio are lower than in common RC structures, which can be attributed to the low contribution of TiABs as they do not fully yield in these specimens. The drastic increment in damping at moderate drifts can be attributed to the concrete damage in each case. In Figure 7(b), it is evident that for specimen U-NS, damping reaches its maximum value at a lateral drift of 2%, followed by a gradual increment until reaching the ultimate drift. For this type of piers, the normal steel fully yielded before the concrete sustained significant damage so the damping was more consistent. Additionally, it can be noted that higher axial loads resulted in reduced damping in this specimen. In addition, the values of equivalent damping for U-NS are similar

to those obtained in conventional RC structures. Thus, it is worth noting that the rate of damping increment is lower in specimens with TiABs than the specimens with normal steel.

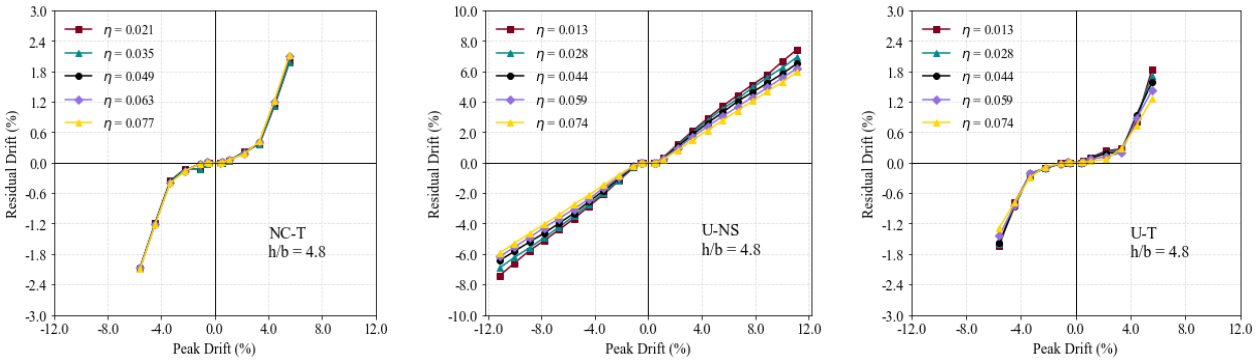

(a) (b) (c)

Figure 6: Influence of axial load on residual drifts in (a) NC-TI, (b) U-NS, and (c) U-TI specimens.

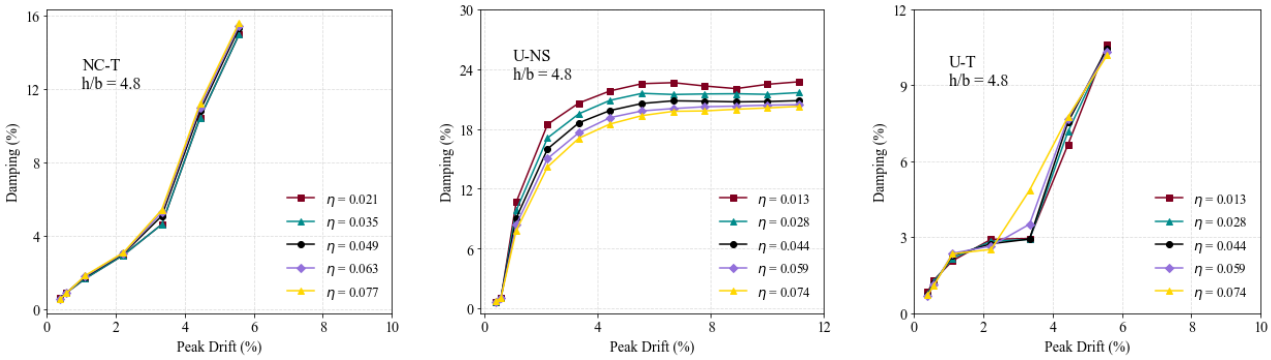

(a) (b) (c)

Figure 7: Influence of axial load on equivalent damping of (a) NC-TI, (b), U-NS, and (c) U-TI specimens.

4.2 Influence of aspect ratio

To evaluate the influence of the aspect ratio on residual drifts, the heights of each pier were modified to 610, 800, 985, 1200, and 1400 mm so the corresponding aspect ratios *L/D* are 3.00, 3.94, 4.85, 5.91, and 6.89. Figure 8 indicates the residual drifts with increments of the peak drift for the three types of piers. As shown in Figure 8(a) and (c), at a constant level of lateral drift, larger residual drifts were noted in specimens NC-TI and U-TI for cases with lower values of *L/D*. This can be attributed to the behavior of TiABs, for larger values of *L/D* the corresponding flexural moments introduce larger stresses in the reinforcement and allow more dissipation of energy. In addition, for lower values of *L/D*, the shear deformations are more important. A similar trend can be noted for the U-NS pier (see Figure 8(b)); however, the influence of *L/D* on the residual drifts is less notorious. From all the types of piers, the U-TI (TARUHPC pier) sustained the smallest residual drifts at a given peak drift and a given value of *L/D*.

Figure 9 shows the variation of the equivalent damping ratio with lateral drifts for the three types of piers. As shown in Figure 9(a) and (c), for the same peak drift, the damping ratio in piers NC-TI and U-TI is higher for lower values of *L/D*. Moreover, the peak drift at which the damping drastically increases is lower for lower values of *L/D*. This can be attributed to the actions in the TiABs as they sustain larger stresses in more slender piers, preventing the early concrete damage observed in piers with lower *L/D*. As noted in Figure 9(b), the damping in U-NS reduces with increments of *L/D*, but this effect is less drastic. For U-NS, the damping

increases rapidly from a drift of 0% to 2% and then increases slowly until reaching the maximum peak drift. This can be attributed to the early onset of yielding on the normal steel of this type of piers, which keeps a stable energy dissipation. Among all the types of piers, U-NS provided the largest damping at a given drift and *L/D*.

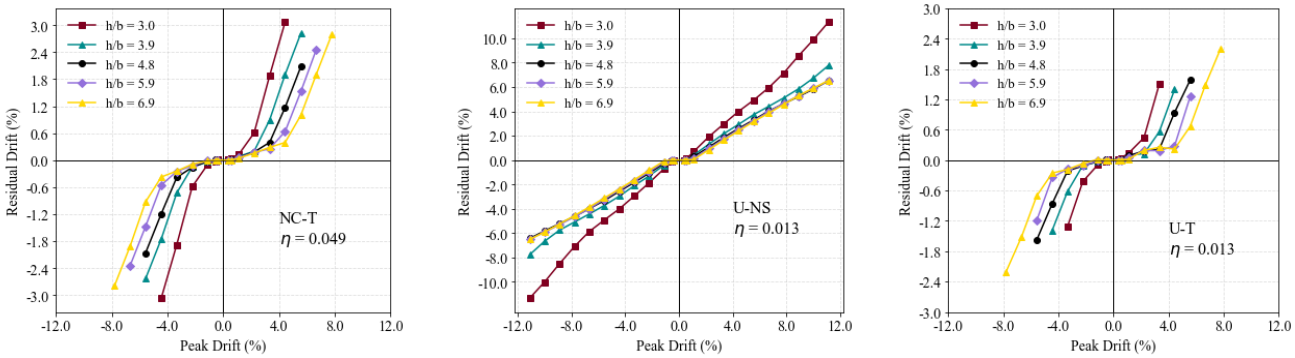

(a) (b) (c)

Figure 8: Influence of aspect ratio on residual drifts in (a) NC-TI, (b) U-NS, and (c) U-TI specimens.

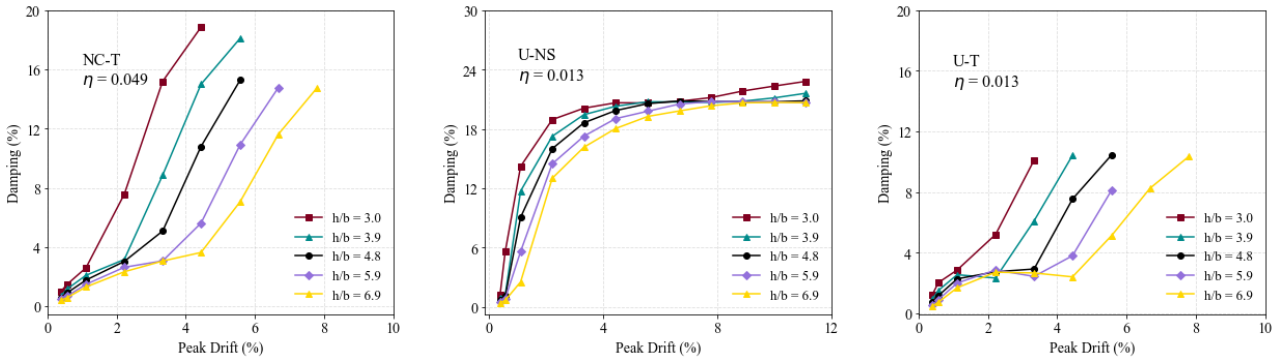

(a) (b) (c)

Figure 9: Influence of aspect ratio on equivalent damping of (a) NC-TI, (b) U-NS, and (c) U-TI specimens.

4.3 Influence of longitudinal reinforcement ratio

The longitudinal reinforcement ratio (ρ) was also evaluated and different values of ρ were applied to the previously studied piers. For NC-TI and U-TI piers the values of ρ were 0.71%, 1.29%, 1.99%, 2.84%, and 3.87%. For the U-NS pier, the values of ρ were 1.07%, 1.94%, 2.99%, 4.26%, and 5.81%. Figure 10 illustrates the residual drifts with increments of the peak drift for the three piers. Figure 10(a) and (c) show that piers NC-TI and U-TI exhibit similar trends in which residual drifts are low (close to 0%) when the drift is less than 3%, followed by a drastic increment of drift ratios. Furthermore, it can be observed that the larger values of ρ slightly increase the values of residual drifts and the drift at which the drastic change in residual drifts occurs. This can be attributed to the fact that TiABs are not reaching their full yield capacity in these piers, so adding more reinforcement increases rapidly the compressive deformations on the section (over-reinforced section) and accelerates the early damage on the concrete. As for pier U-NS, Figure 10(b) shows that the residual drift ratio increases rapidly with the increment of the peak drift ratio, this phenomenon indicates that the reinforcing bars reach early their yield stress and the deformation is controlled by the strength in the reinforcing. Moreover, it is noted that a higher reinforcement ratio correlates with a higher residual displacement.

Figure 11 indicates the influence of different reinforcing ratios on the equivalent viscous damping of the piers. Figure 11(a) shows that reinforcing bars do not have a significant effect

on the damping ratio for NC-TI, which can be attributed to the early damage of concrete as the reinforcement does not reach its full strength. For U-TI piers (see Figure 11(c)), the damping slightly reduces for larger values of ρ, which can be attributed to the difficulty in reaching the yield strength in piers with larger amounts of TiABs. As for U-NS piers, the damping increases with increments of ρ (see Figure 9(b)). Moreover, it is evident that for U-NS piers, damping reaches its maximum value at a lateral drift of about 2%, followed by a slow increment until reaching the ultimate drift of 11%. Since the behavior of U-NS piers is governed by the yielding of normal steel, adding more reinforcement dissipates more energy.

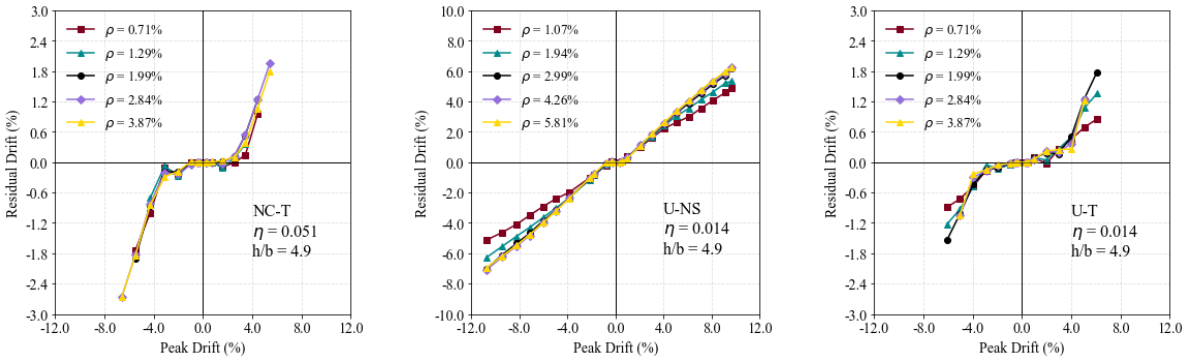

(a) (b) (c)

Figure 10: Influence of longitudinal reinforcement on residual drifts in (a) NC-TI, (b) U-NS, and (c) U-TI.

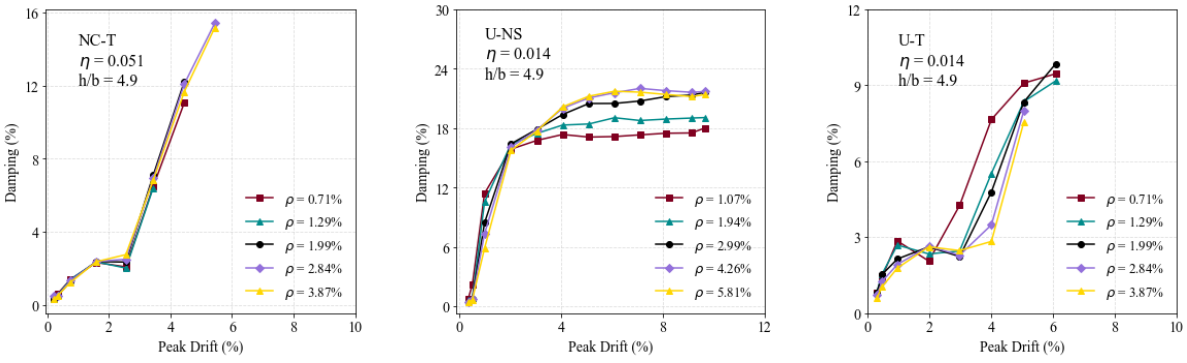

(a) (b) (c)

Figure 11: Influence of longitudinal reinforcement on equivalent damping of (a) NC-TI, (b) U-NS, and (c) U-TI.

5 DESIGN RECOMMENDATIONS

Based on the results of the parametric study, design recommendations are provided for TARUHPC structures. In particular, recommendations to control residual drifts are provided. Residual drifts are commonly associated with the seismic resilience capacity of bridges, so it is important to control residual drifts. The Japan Road Association code [14] recommends that residual drifts of RC bridge piers should be below 1.0% so that bridges can be repairable. Furthermore, Saiidi et al [15] suggest values of residual drift of 1.0% and 1.5%, to distinguish between low, moderate, and high levels of damage. Figure 12 shows the residual drift vs peak drift for all the FE models considered in the parametric analysis. At a given level of lateral drift, the U-TI piers (TARUHPC bridges) sustained lower residual drifts than the other cases. For instance, as shown in Figure 12(a), in order to reach a residual drift lower than 1.0% the lateral drift of the specimen NC-TI should be limited to around 2.5%. As for specimen U-NS (see Figure 12(b)), the lateral drift should be limited to around 2% to keep the residual drift below 1%. On the contrary, the specimen U-TI can sustain lateral drifts up to 4% with residu-

al drifts below 1.0%. These drift limits aim to keep the bridges repairable after a major earthquake event. As noted with these results, the combination of UHPC and TiABs can help in reducing residual drifts, increasing the seismic resilience of bridges.

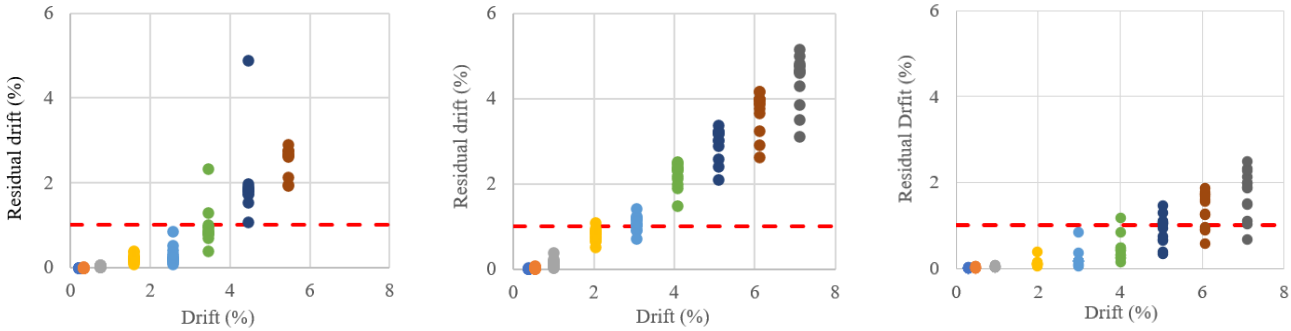

Figure 12: Residual drift and peak drift of (a) NC-TI, (b) U-NS, and (c) U-TI specimens.

6 CONCLUSIONS

A comprehensive numerical evaluation of the cyclic behavior of columns with UHPC, NC, NS, and TiABs was conducted. Different design parameters were evaluated numerically and the following conclusion can be drawn:

- The numerical models proposed in this paper were able to capture the seismic performance of bridge piers using UHPC and TiABs.
- For NC-TI and U-TI piers, TiABs did not achieve their full yielding during most of the loading, so the energy dissipation and strength were controlled by the damage in the concrete. The UHPC in U-TI allowed the TiAB to reach more tensile stresses.
- U-TI piers (TARUHPC) had more strength and deformation capacity than NC-TI; however, it showed lower damping than specimens U-NS.
- The axial load has some influence on the residual damage and energy dissipation of U-NS piers, but this influence was minimal for NC-TI and U-TI.
- In order to keep bridges repairable after a major earthquake (residual drifts), the lateral drifts of NC-TI, U-NS, and U-TI should be limited to 3%, 2%, and 4%, respectively.
- Experimental and numerical results showed that TARUHPC can be helpful in reducing the residual drifts on bridge piers, thus improving the seismic resilience of bridges.

REFERENCES

[1] A. Al-Ostaz, *Diagnostic evaluation, and repair of deteriorated concrete bridges. Mississippi Department of Transportation*, Oxford, MS, USA, Final. Rep. FHWA/MS-DOT-RD-04-169. 2004. Available: https://trid.trb.org/view/753672

[2] ARTBA, *ARTBA Bridge Report*, American Road & Transportation Builder Association. 2024. Available: https://artbabridgereport.org/

[3] M. Acharya, L.A. Bedriñana, J. Cantrell, & M. Mashal, Revolutionary Construction Approach for Civil and Critical Infrastructures: Titanium Alloy Rein-forced Ultra-High Performance Concrete (TARUHPC). *1st GCC Engineering Symposium 2023*, Kuwait City, Kuwait. 2023.

[4] M. Acharya, L.A. Bedriñana, & M. Mashal, Experimental and Data-Driven Evaluation of the Bond Strength between UHPC and Titanium Alloy Reinforcing Bars. *Structures*, Accepted for publication. 2025.

[5] R. Khadka, M. Acharya, & J. Cantrell, Experimental Investigation on Mechanical Properties of Titanium Alloy Bars: Comparison with High-Strength Steel. *Special Publication of American Concrete Institute*, 341 (8), 160-187. 2020.

[6] M. Acharya, R. Khadka, & M. Mashal, Preliminary Bond Testing and Splicing of Titanium Alloy Bars. *Transportation Research Record*, 2676(5), 410–427, 2022. https://doi.org/10.1177/03611981211067785

[7] J. Li, Z. Wu, C. Shi, Q. Yuan, & Z. Zhang, Durability of ultra-high performance concrete-A review, *Construction and Building Materials*, 25 (119296), 2020. doi: https://doi.org/10.1016/j.conbuildmat.2020.119296.

[8] J. Du et al., New development of ultra-high-performance concrete (UHPC). *Composites Part B: Engineering*, 224 (109220), 2021. doi: https://doi.org/10.1016/j.compositesb.2021.109220

[9] C. Wu, J. Li, Y. Su, Development, testing, and numerical simulation of ultra-high performance concrete at material level, *in Development of Ultra-high Performance Concrete against Blasts*. Cambridge, MA: Woodhead Publishing Series in Civil and Structural Engineering, 2018. doi: https://doi.org/10.1016/B978-0-08-102495-9.00002-5

[10] M. Acharya, J. Cantrell, L.A. Bedriñana, & M. Mashal, Experimental research on durable and seismic-resilient concrete bridges with use of novel materials. *18th World Conference on Earthquake Engineering*. Milan, Italy, June 30th – July 5th, 2024.

[11] F.T. McKenna, Object-oriented finite element programming: frameworks for analysis, algorithms, and parallel computing. *Ph.D. dissertation*, University of California, Berkeley, CA. 1997.

[12] D. Kent, R. Park, Flexural members with confined concrete. *Journal of the structural division*, 97 (7), 1969-1990, 1971. doi: https://doi.org/10.1061/JSDEAG.0002957

[13] J. B. Mander, M. J. N. Priestley, & R. Park, Theoretical Stress ‐ Strain Model for Confined Concrete. *Journal of Structural Engineering*, 114(8), 1804 ‐ 1826, 1988. doi: https://doi.org/10.1061/(ASCE)0733-9445(1988)114:8(1804)

[14] Z. Wang, J. Wang, T. Liu, & F. Zhang, Modeling seismic performance of high-strength steel-ultra-high-performance concrete piers with modified Kent-Park model using fiber elements. *Advances in Mechanical Engineering*, 8 (2), 1-14, 2016. doi: https://doi.org/10.1177/1687814016633411

[15] A. Zsarnoczay, Experimental and Numerical Analysis of Buckling Restrained Braced Frames for Eurocode Conform Design Procedure Development. *PhD Thesis*. Budapest University of Technology and Economics, Budapest, Hungary, 2013.

[16] Japan Road Association, *Specifications for highway bridges-Part V Seismic design*. Marusan Publishing, Tokyo, Japan, 2002.

[17] M.S. Saiidi, M. Tazarv, S. Varela, S. Bennion, M.L. Marsh, & I. Ghorbani, *Seismic evaluation of bridge columns with energy dissipating mechanisms*. NCHRP Research Report 864, Washington (DC), The National Academics Press. 2017.